

## THE MASS-METALLICITY RELATION FOR GIANT PLANETS

DANIEL P. THORNGREN<sup>1</sup>, JONATHAN J. FORTNEY<sup>2</sup>, AND ERIC D. LOPEZ<sup>3</sup>

(Dated:)  
Draft version April 20, 2022

### ABSTRACT

Exoplanet discoveries of recent years have provided a great deal of new data for studying the bulk compositions of giant planets. Here we identify 38 transiting giant planets ( $20M_{\oplus} < M < 20M_J$ ) whose stellar insolation is low enough ( $F_* < 2 \times 10^8 \text{ erg s}^{-1} \text{ cm}^{-2}$ , or roughly  $T_{\text{eff}} < 1000$ ) that they are not affected by the hot Jupiter radius inflation mechanism(s). We compute a set of new thermal and structural evolution models and use these models in comparison with properties of the 38 transiting planets (mass, radius, age) to determine their heavy element masses. A clear correlation emerges between the planetary heavy element mass  $M_z$  and the total planet mass, approximately of the form  $M_z \propto \sqrt{M}$ . This finding is consistent with the core accretion model of planet formation. We also study how stellar metallicity  $[\text{Fe}/\text{H}]$  affects planetary metal-enrichment and find a weaker correlation than has been previously reported from studies with smaller sample sizes. Our results suggest that planets with large heavy element masses are more common around stars with a high iron abundance, but are not found there exclusively. We confirm a strong relationship between the planetary metal-enrichment relative to the parent star  $Z_{\text{planet}}/Z_{\text{star}}$  and the planetary mass, but see no relation in  $Z_{\text{planet}}/Z_{\text{star}}$  with planet orbital properties or stellar mass. Suggestively, circumbinary planets are more enriched in heavy elements than similar mass single-star planets, but with only four such planets the effect is not yet significant. The large heavy element masses of many planets ( $> 50 M_{\oplus}$ ) suggest significant amounts of heavy elements in H/He envelopes, rather than cores, such that metal-enriched giant planet atmospheres should be the rule.

### 1. INTRODUCTION

Giant planets do not directly take on the composition of their parent stars. If some flavor of core-accretion formation is correct (Pollack et al. 1996), then a seed core of  $\sim 5-10M_{\oplus}$  of ice/rock must build up first, which begins accreting nebular gas. The gas need not share the exact composition of the parent star, due to condensation and migration of solids within the disk (Lodders 2009; Öberg et al. 2011). The growing giant planet accretes gas but is also bombarded by planetesimals, which may add to the core mass or dissolve into the growing H/He envelope. The amounts and variety of heavy elements (metals) accreted by the growing planet will depend on its formation location, formation time, disk environments sampled, and whether it forms near neighboring planets, among many other factors. A planet's present-day composition is our indirect window into its formation process.

Within the Solar System, the non-Solar composition of our giant planets can be observed in two complementary ways. The observed atmospheric composition of fully convective giant planets provides the mixing ratios of heavy elements within the whole H/He envelope, which is nearly  $300 M_{\oplus}$  in Jupiter. Spectroscopy of the Solar System's giants points to enhancements in the mixing ratio of carbon (as seen in  $\text{CH}_4$ ) of  $\sim 4$ , 10, 80, and 80, in Jupiter, Saturn, Uranus, and Neptune, respectively (Wong et al. 2004; Fletcher et al. 2009). The *Galileo Entry Probe* found that Jupiter's atmosphere is enhanced in volatiles like C, N, S, and noble gases by factors of 2-5 compared to the Sun (Wong et al. 2004).

Remarkably, one can infer the *bulk* metallicity, or heavy element enhancement,  $Z_{\text{planet}}/Z_{\text{Sun}}$ , of a Solar System giant

planet by measuring only its mass and radius. By comparing to structure models, it is straightforward to infer from mass and radius alone that Jupiter and Saturn are both smaller and denser than they would be if they were composed of solar composition material (Zapolsky & Salpeter 1969; Fortney et al. 2007). Therefore, we can infer they are enhanced in heavy elements. As we describe below, this leads to an immediate connection with transiting giant planets, where mass and radius can be accurately measured.

Knowledge of the heavy element enrichment of our Solar System's giant planets has led to dramatic advances in our understanding of planet formation. Models of the core-accretion model of planet formation have advanced to the point where they can match the heavy element enrichment of each of the Solar System's giant planets (Alibert et al. 2005; Lissauer et al. 2009; Helled & Bodenheimer 2014). However, we are only beginning to attain similar data for exoplanets, which will provide a critical check for planet formation models over a tremendously larger phase space. Such constraints are particularly important for comparison with planetary population synthesis models that aim to understand the processes of core formation, H/He envelope accretion, and planetary migration, in diverse protoplanetary environments (Ida & Lin 2004; Mordasini et al. 2014). Constraints on planet formation from exoplanetary systems have been almost entirely driven by data on the frequency of planets in the mass/semi-major axis plane. A promising avenue is to move these comparisons into a complementary plane, that of planetary composition, either in bulk composition (Guillot et al. 2006; Burrows et al. 2007; Miller & Fortney 2011; Mordasini et al. 2014), or atmospheric composition (Madhusudhan et al. 2011; Fortney et al. 2013; Kreidberg et al. 2014; Barman et al. 2015; Konopacky et al. 2013) as shown in a schematic way in Figure 1.

The dramatic rise in the number of observed transiting exoplanets provides a unique opportunity. With radii derived from transit observations and masses derived from radial-

<sup>1</sup> Department of Physics, University of California, Santa Cruz, USA

<sup>2</sup> Department of Astronomy and Astrophysics, University of California, Santa Cruz, USA

<sup>3</sup> Institute for Astronomy, Royal Observatory Edinburgh, University of Edinburgh, Blackford Hill, Edinburgh, UK

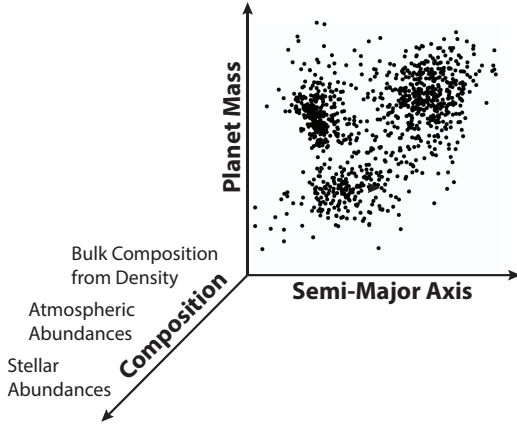


FIG. 1.— A highly schematic and simplified view of planes useful for understanding planet formation. The main purpose of this study is to provide planetary composition information to inform planet formation models.

velocity or transit-timing variation measurements, we get especially detailed information about these objects. This gives us a measured density, and therefore some rough information about their bulk composition. A more advanced analysis uses models of planet structural evolution (e.g. Fortney et al. (2007)) to constrain the quantity of heavy elements.

Most of the giant planets we have observed are strongly irradiated hot Jupiters, whose radii are inflated beyond what models predict. Much effort has been put into understanding this discrepancy. A thorough discussion is outside the scope of this paper, but the various proposed inflation mechanisms are extensively reviewed in Fortney & Nettelmann (2010), Baraffe et al. (2014), and Weiss et al. (2013). Unfortunately, without a definite understanding of the inflation process this acts as a free parameter in modeling: the inflationary effect enlarges a planet and added heavy elements shrink it, resulting in a degeneracy that inhibits our ability to obtain useful composition constraints. Still, work has been done to use models to address the star-planet composition connection, using plausible assumptions about the effect, as a heat source (Guillot et al. 2006) or as a slowed-cooling effect (Burrows et al. 2007). Both studies saw an increase in planet heavy element mass with stellar metallicity.

A promising avenue of investigation are the sample of tran-

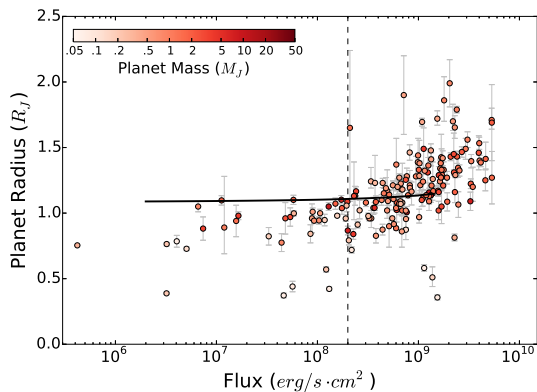


FIG. 2.— Planetary radii for observed planets against stellar insolation. The black line is an 4.5 Gyr,  $1 M_J$  pure H/He object, roughly the maximum radius for older, uninflated planets. The dashed vertical line marks the flux cutoff we use to identify the cool, uninflated giants.

siting exoplanets which are relatively cool. Planets that receive an incident flux below around  $2 \times 10^8 \text{ erg s}^{-1} \text{ cm}^{-2}$  ( $T_{\text{eq}} \lesssim 1000 \text{ K}$ ) appear to be non-inflated (Miller & Fortney 2011; Demory & Seager 2011), obviating the need for assumptions about that effect. Figure 2 shows this threshold. Miller & Fortney (2011) (hereafter referred to as MF2011) studied these planets, finding correlations in the heavy element mass with planetary mass and stellar metallicity. In particular, they noted a strong connection between the relative enrichment of planets relative to their parent stars ( $Z_{\text{planet}}/Z_{\text{star}}$ ) and the planet mass. However, that study was limited by a small sample size of 14 planets.

In our work that follows, we consider the set of cool transiting giant planets, now numbering 38, and compare them to a new grid of evolution models to estimate their heavy element masses, and we include a more sophisticated treatment of the uncertainties on our derived planetary metal-enrichments. We then examine the connections between their mass, metal content, and parent star metallicity.

## 2. PLANET DATA AND SELECTION

Our data was downloaded from the Extrasolar Planets Encyclopedia (exoplanets.eu, Schneider et al. 2011) and the NASA Exoplanet Archive (Akeson et al. 2013). These data were combined, filtered (see below) and checked against source papers for accuracy. Some corrections were needed, mostly in resolving differing values between papers; we aimed to consistently use the most complete and up-to-date paper. We tried to include all known planets who met the selection (even if some of their data was found in the literature and not the websites). Critically, we use data from the papers we source, rather than the websites (see Table 1).

For our sample, we selected the cool giant planets that had well-determined properties. Typically, this means they were the subject of both transit and radial velocity studies. The mass and radius uncertainties were of particular importance. Planets needed to have masses between  $20M_{\oplus}$  and  $20M_J$ , and relative uncertainties thereof below 50%. Our sample's relative mass uncertainties were typically well below that cutoff, distributed as  $10^{+11.8}_{-4.9}\%$ . We also constrained relative radius uncertainty to less than 50%, but again saw values much lower ( $10.4^{+7.9}_{-4.7}\%$ ). Both uncertainty cuts were made to eliminate planets with only rough estimates or upper limits for either value.

As discussed in §1, we used a  $2 \times 10^8 \text{ erg s}^{-1} \text{ cm}^{-2}$  upper flux cutoff to filter out potentially inflated planets. Consequently, candidates needed to have enough information to compute the flux: stellar radius and effective temperature (for both stars, if binary), semi-major axis, and eccentricity. In addition, we needed measured values for the stellar metallicities in the form of the iron abundance [Fe/H]. These tended to have fairly high uncertainties, and were a major source of error in our determination of  $Z_{\text{planet}}/Z_{\text{star}}$ .

Determining the age of a planet is necessary to use evolution models to constrain its metal content; unfortunately, this is often a difficult value to obtain. Our ages come from stellar ages listed in the literature, typically derived from a mixture of gyrochronology and stellar evolution models. These methods can produce values with sizable uncertainties, typically given as plausible value ranges. We treat these as flat probability distributions (a conservative choice), and convert values given as Gaussian distributions to 95% confidence intervals.

Because planets do most of their cooling, and therefore con-

traction, early in their lives (see Fortney et al. 2007, for a discussion), large uncertainties in age are not a major obstacle in modeling older planets. For planets who may be younger than a few Gyr, we cannot rule out that they are very metal-rich, but young and puffy, as the two effects would cancel out. We account for this in our analysis; planets which may be young consequently exhibit higher upper bound uncertainties in heavy element mass. For Kepler-16 (AB)-b, Kepler-413 (AB)-b, and WASP-80 b, no age was given, so we used a range of .5-10 Gyr. This is reasonable because it represents the possibilities of the planets being either young or old, and because the age was a second-order effect on our heavy element assessment (after mass and radius).

### 3. MODELS

We created one-dimensional planetary models consisting of an inert core composed of a 50/50 rock-ice mixture, a homogenous convective envelope made of a H/He-rock-ice mixture, and a radiative atmosphere as the upper boundary condition. The models are made to satisfy the equations of hydrostatic equilibrium, mass conservation, and the conservation of energy.

$$\frac{\partial P}{\partial m} = -\frac{Gm}{4\pi r^4} \quad (1)$$

$$\frac{\partial r}{\partial m} = \frac{1}{4\pi r^2 \rho} \quad (2)$$

$$\frac{\partial L}{\partial m} = -T \frac{\partial S}{\partial T} \quad (3)$$

Equation 3 is not used in the core, where luminosity is neglected. Structures are initially guessed, then iteratively improved until these conditions are met to within sufficiently small error. This computation was done in a new Python code created for this study. Its advantages are its relative speed (a 6 million planet grid takes < 1 hour to create) and its ability to easily try different compositional structures (e.g. heavy elements in the core vs. envelope) and/or equations of state.

For our atmosphere models, we interpolate on the solar metallicity grids from Fortney et al. (2007), as was done in several other papers (including Miller et al. (2009) and Lopez & Fortney (2014)). With these models we compute the intrinsic luminosity ( $L$ ) of a planet model (see equation 3), which describes the rate that energy escapes from the interior, at a given surface gravity and isentropic interior profile. These grids are then used to determine the rate of entropy change in the envelope, and the contraction history of a given model planet. The initial entropy is not important; reasonable initial values typically all converge within a few hundred million years (Marley et al. 2007). As such we do not need to consider if planets form in a hot or cold start scenario. Following Miller et al. (2009), we include the small extension in radius due to the finite thickness of the radiative atmosphere. A fully self-consistent treatment of the atmosphere would use a range of metal-enriched atmosphere grids to be interpolated to yield consistency between atmospheric metallicity and H/He envelope metal mass fraction. Metal-enriched grids would tend to slow cooling and contraction (Burrows et al. 2007) and yield *larger* heavy element masses than we present here. However, given uncertainties in the upper boundary condition in strongly irradiated giant planets (e.g., Guillot 2010; Spiegel & Burrows 2013), and our uncertainty in where the heavy el-

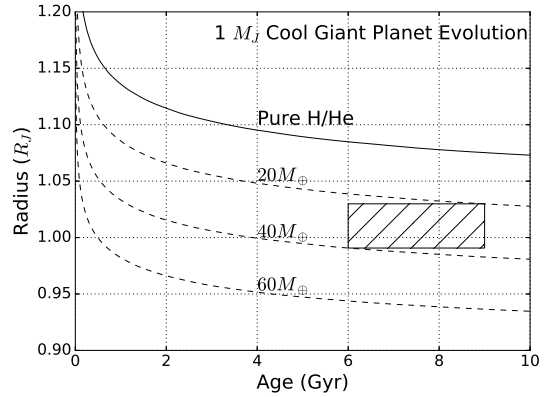


FIG. 3.— The radius evolution over time of  $1 M_J$  planets with low stellar insolation ( $1 \times 10^7 \text{ erg s}^{-1} \text{ cm}^{-2}$ ) containing various quantities of metal. The box is a simple example of how to determine the metal content. We infer that a cool  $1 M_J$  planet with an observed age of 6-9 Gyr and radius of  $0.99 - 1.03 R_J$  has 20-40  $M_{\oplus}$  of heavy elements. The system we used handles uncertainties in a more advanced way: see §4 for details.

ements are within the planets (core vs. envelope) it is not clear if such an expanded study is yet warranted.

In creating our models, we had several important factors to consider: where the heavy elements are within the planet, what the composition of these heavy elements is, and how to treat the thermal properties of the core. These questions do not have any clearly superior or well-established solutions. The uncertainties from them, however, were overshadowed by the large uncertainties from available values for mass, radius and (to a lesser extent) age. Therefore, in designing our models, we chose plausible solutions instead of attempting to incorporate all modeling uncertainties into our results.

#### 3.1. Heavy Element Distribution

Hydrogen-Helium mixtures are more compressible than typical heavy elements, and so models with heavy elements in a core tend to be larger than models with the same heavy element mass mixed throughout the envelope (see Baraffe et al. 2008, for a discussion). Conversely, modeling planets with pure heavy element cores and pure H/He envelopes requires the most heavy elements of any structure for a given total mass and radius. For some planets in our sample we find this kind of model requires implausibly high metal-enrichment to explain a given radius (cores of several *Jupiter masses* for extreme cases), and it is difficult to imagine how such massive cores could form. As such, in our models here we distribute the heavy element mass by putting up to  $10 M_{\oplus}$  into a pure heavy element core, and then use linear mixing to put any remaining metal mass in the otherwise H/He envelope. This allows us to consistently model both core-dominated low-mass planets and likely better-mixed massive planets.

#### 3.2. Equations of State

For hydrogen and helium we used the Saumon et al. (1995) equation of state (EOS), with a solar ratio of hydrogen to helium ( $Y = 0.27$ ). For envelopes with metals mixed in, we used additive volumes to adjust the equation of state. Our choice for the metal EOS was also important – denser materials like iron produce noticeably smaller planets (and therefore require a smaller  $Z_{\text{planet}}$  to explain a given planet). Olivine, a mineral whose EOS is commonly used to represent rock, is less dense than iron. Water, used as a proxy for ices generally, is less

dense still. MF2011 showed that changing the metal composition produces differences on the order of 20%, consistent with our models. We chose to use a 50-50 rock-ice mixture, using the Thompson (1990) ANEOS equation of state. This would overestimate  $Z_{\text{planet}}$  if the metal were actually iron-dominated, but this seems unlikely to occur commonly in giant planets, which are typically expected to form near the snow line (Ida & Lin 2004).

#### 4. ANALYSIS

To apply our models to an observed planet, we generate sample planets using the distributions from observational uncertainty in mass, radius, age, and stellar metallicity. Each sample planet is assigned a value for these from the distributions. These distributions are Gaussian, except for the age which is conservatively modeled as a flat range (see §2). The sample planets are then paired with a model interpolated from our grid to assign values of heavy element mass,  $Z_{\text{planet}}$ , and  $Z_{\text{planet}}/Z_{\text{star}}$ .

The resulting heavy element mass distributions were single peaked and roughly Gaussian overall (see Figure 4), but sometimes correlated strongly with mass for planets with high  $Z_{\text{planet}}$  and with radius for those with low  $Z_{\text{planet}}$ . Our reported values show the mean of each distribution, with uncertainties computed as the standard deviation of samples above the mean and below the mean. These represent the data reasonably well, but care should be taken not to overlook the correlation with input variables. For our part, we do all computation directly on the samples (see below), and report the uncertainties in the resulting distributions.

Some planets whose  $Z_{\text{planet}}$  values were clustered near zero (pure H/He) or one (pure ice/rock) generated samples which could not be recreated in our models. (For instance,  $Z_{\text{planet}} = 0$  could occur if the sample is randomly assigned a low value for mass and a high value for its radius, and ends up being larger than an analogous pure H/He object). These samples were discarded, but we noted how often this occurred. For the six planets where this occurred 15.8% - 50% of the time (where at least a  $1\sigma$  tail is outside the valid range), the error-bar on that side was adjusted to a  $Z_{\text{planet}}$  of exactly 0 or 1, as appropriate. These are marked with a † in Table 1. For the massive H/He dominated planet Kepler-75b, this occurred more than half the time, so its heavy element derived values are listed as upper limits.

To conduct the regressions described in our results (§5), we use statistical bootstrapping. One sample was randomly chosen from the set for each planet, and regression was done on this sub-sample ‘scenario’. This was done repeatedly to generate a distribution of results. Since the samples reflect observational uncertainty, the distribution of the fit parameters do as well. Note that the uncertainties in our results still do not take modeling error into account. Our use of this method is justified because the implicit assumption – that each sub-sample is independent of the others – is made trivially true by ensuring that we take exactly one sample per planet into each considered sub-sample (each planet is independent of the others). We chose this solution because it allows us to account for correlations between values (e.g. mass and heavy element mass for high  $Z_{\text{planet}}$  planets) without resorting to complex analytical approximations of the distributions. The best alternative technique appears to be hierarchical Bayesian modeling, which would require substantially more work to implement, but with little gains in insight. Fortunately, we can construct our sub-samples to be independent and our mod-

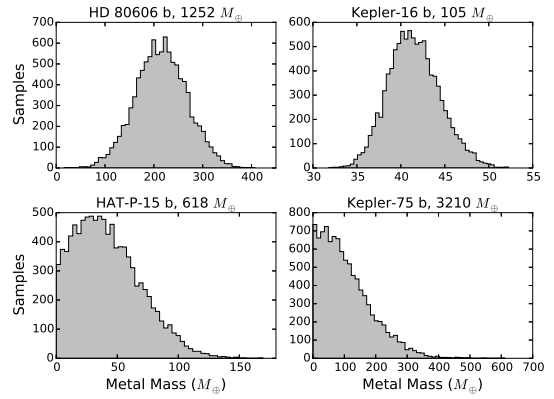


FIG. 4.— Histograms of the posterior heavy element masses for four giant planets, with 10,000 samples each. The top two, HD 80606b and Kepler-16b, have distributions typical of the sample. HAT-P-15b is one of the six planets for which more than a  $1\sigma$  portion of the distribution extends below the pure H/He limit. Each of these planets has had their lower error bars extended to zero, changes marked with a † in Table 1. Kepler-75b is the single planet for which only an upper limit could be determined; its RMS heavy element mass ( $134 M_{\oplus}$ ) is reported as the upper error.

els follow a simple structure ( $M, R, F, \text{Age}, [Fe/H] \rightarrow M_z, Z_{\text{planet}}, Z_{\text{planet}}/Z_{\text{star}} \rightarrow \text{Estimators}$ ), so the results from either procedure should be comparable.

We considered the possibility that mass and radii observations are not independent. If they are correlated, then sampling more directly from observational data (or posteriors thereof) could improve the uncertainties in our heavy element masses. Such an operation would need to be careful not to assume the results we are trying to derive. Southworth et al. (2007) describes a method of computing surface gravity which is more precise than directly using a planet’s derived mass and radius. They instead use orbital parameters, the planet’s radius, and the stellar reflex velocity  $K$ . These are closer to the observed quantities, and so avoid unnecessarily compounding uncertainties. We used Southworth’s formula as a proxy to estimate how much improvement in uncertainty we might see from such an approach. We found that most of our planets exhibited only modestly better gravity estimates (though a handful were substantially improved, such as HAT-P-18 b). As such, we determined that trying to work more directly from observation data would not be worthwhile for our set of planets. Still, we suggest that studies examining individual planets should consider this approach.

## 5. RESULTS

We examined our results for connections between three quantities connected through the core-accretion model: the planetary mass  $M$ , its heavy element mass  $M_z$ , and the stellar metallicity  $[Fe/H]$ . We also considered the metal mass fraction of the planet  $Z_{\text{planet}}$  and its ratio to that of the parent star  $Z_{\text{planet}}/Z_{\text{star}}$ .

### 5.1. Relation to Planet Mass

There exists a clear correlation between planet mass and heavy element content. We can see that as we move towards more massive planets, the total mass of heavy elements increases, but the bulk metallicity decreases (Figure 5). This is consistent with a formation model where an initial heavy element core accretes predominantly, but not exclusively, H/He gas (e.g. Pollack et al. (1996)). Indeed, we see a minimum heavy element mass at around  $5 - 10 M_{\oplus}$ , agreeing with both

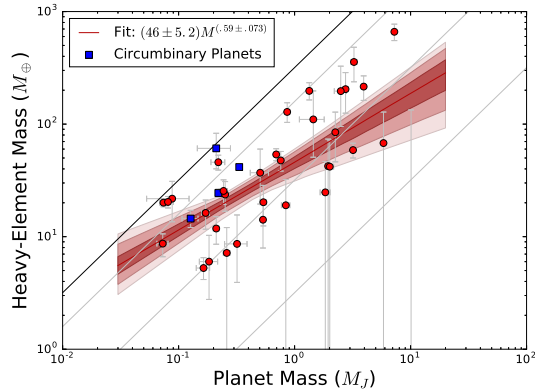


FIG. 5.— The heavy element masses of planets and their masses. The lines of constant  $Z_{\text{planet}}$  are shown at values of 1 (black), 0.5, 0.1, and .01 (Gray). Distributions for points near  $Z_{\text{planet}} = 1$  tend to be strongly correlated (have well-defined  $Z_{\text{planet}}$  values) but may have high mass uncertainties. No models have a  $Z_{\text{planet}}$  larger than one. The distribution of fits (see §4 for discussion) is shown by a red median line with 1, 2, and 3  $\sigma$  contours. Blue squares indicate circumbinary planets. Note Kepler-75b at  $10.1 M_J$  which only has an upper limit.

MF2011 and theoretical core-formation models (Klahr & Bodenheimer 2006). A bootstrap power-law fit to the data gives  $M_z = (46 \pm 5.2)M^{(.59 \pm .073)}$ , or roughly  $M_z \propto \sqrt{M}$  and  $Z_{\text{planet}} \propto 1/\sqrt{M}$ . Our parameter uncertainties exclude a flat line by a wide margin, but the distribution has a fair amount of spread around our fit. While some of this may be from observational uncertainty, it seems likely that other effects, such as the planet’s migration history and the stochastic nature of planet formation, also play a role. With this in mind, using planet mass alone to estimate the total heavy element mass appears accurate to a factor of a few.

We note that the four circumbinary planets in our sample (marked as blue squares in Figure 5) appear to typically have higher heavy-element contents for their mass than the general sample. We examined the residuals to the fit of heavy-elements against mass (this time excluding the circumbinary planets). This was done to control for the effect of the planet’s mass. A K-S test was applied to these residuals, revealing a p-value of 0.26 that the circumbinary planets were drawn from a different sample than the rest. This result is non-significant, possibly due to the small number of circumbinary planets in our sample. Still, the distribution is suggestive of a possible effect, and this test should be repeated when a larger sample becomes available.

### 5.2. Effect of Stellar Metallicity

The metallicity of a star directly impacts the metal content of its protoplanetary disk, increasing the speed and magnitude of heavy element accretion. We examined our data for evidence of this connection. MF2011 observed a correlation for high metallicity parent stars between  $[\text{Fe}/\text{H}]$  and the heavy element masses of their planets (see also Guillot et al. (2006) and Burrows et al. (2007) for similar results from inflated planets). If we constrain ourselves to the fourteen planets in MF2011, we see the same result. However, the relation becomes somewhat murky for our full set of planets (see Figure 6). A bootstrap regression gives  $M_z = (31.4 \pm 3.4) \times 10^{(.48 \pm .047)[\text{Fe}/\text{H}]}$ . Though this appears to show that the points are positively associated, it is clear from Fig. 6 that no line could fit the data effectively. Some of the reason for this may lie with the high observational uncertainty in our

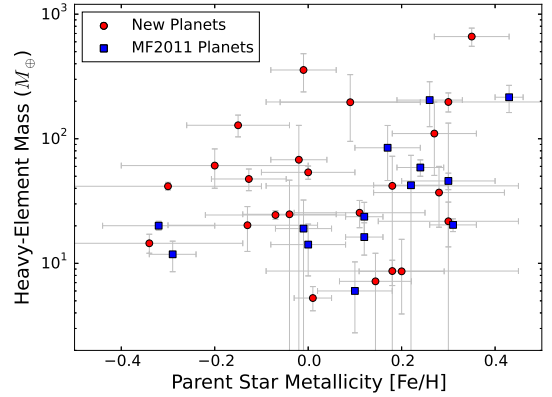


FIG. 6.— The heavy element masses of planets plotted against their parent star’s metallicity. Our results for the planets studied in MF2011 are in blue, and the remaining planets in our data set are in red. A correlation appears for  $[\text{Fe}/\text{H}]$  in the blue points, but washes out with the new data. Still, it appears that planets with high heavy element masses occur less frequently around low iron-metallicity stars.

values for stellar metallicity, but it is still difficult to believe that there is a direct power-law relationship.

A more plausible model is that planets rich in heavy elements are found less frequently around metal-poor stars. Transit surveys should not be biased in stellar metallicity, so this analysis is viable. Most of the planets with heavy element masses above  $100 M_{\oplus}$  orbit metal-rich stars; there is no clear pattern for planets with lower metal masses. Considering the connection between planet mass and heavy element mass, we note that planets more massive than Jupiter are found far less often around low-metallicity stars (see Figure 7). This is similar to one of the findings of Fischer & Valenti (2005) in which the number of giant planets and the total detected planetary mass are correlated with stellar metallicity. The population synthesis models in Mordasini et al. (2012) also observe and discuss an absence of very massive planets around metal-poor stars. Apparently, metal-poor stars generally do not have the massive planets which would typically contain higher metal masses. The causal link for this could be an interesting question for formation and population synthesis models. In the future, a more thorough look at this connection should take into account stellar metal abundances other than iron and put an emphasis on handling the high uncertainties in measurements of stellar metallicity.

### 5.3. Metal Enrichment

A negative correlation between a planet’s metal enrichment relative to its parent star was suggested in MF2011 and found in subsequent population synthesis models (Mordasini et al. 2014), so we revisited the pattern with our larger sample. We see a good relation in our data as well (Figure 9), and a bootstrap fit of  $Z_{\text{planet}}/Z_{\text{star}} = (8.1 \pm 1.3)M^{(-.51 \pm 0.11)}$  cleanly rules out a flat relation. The exponent differs somewhat from the results of Mordasini et al. (2014) (between -0.68 and -0.88), but the discrepancy is not especially large. The pattern appears to be somewhat stronger than if we considered only the planetary metal fraction  $Z_{\text{planet}}$  alone (shown in Figure 8). This supports the notion that stellar metallicity still has some connection to planetary metallicity, even though we do not observe a power-law type of relation. Jupiter and Saturn, shown in blue, fit nicely in the distribution. Our results show that even fairly massive planets are enriched relative to their parent stars. This is intriguing, because it suggests that (since

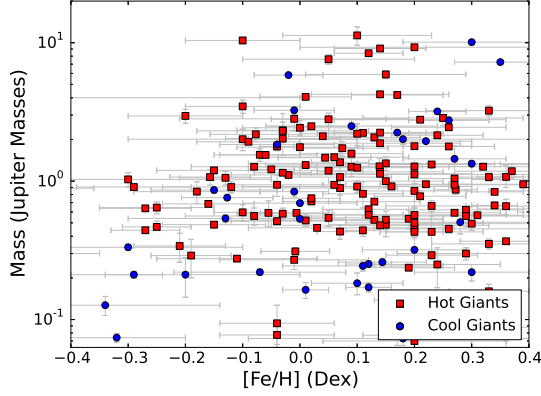


FIG. 7.— Planet mass plotted against parent star metallicity for transiting planets with RV masses. Planets in our sample are in blue. Planets in red were too strongly insolated to pass the flux cut (the inflated hot Jupiters). Note the lack of planets around low-metallicity stars above about  $1 M_J$ . This, combined with the findings on Figure 6, suggests that planets around low-metallicity stars are unable to generate the giant planets which typically have massive quantities of heavy elements.

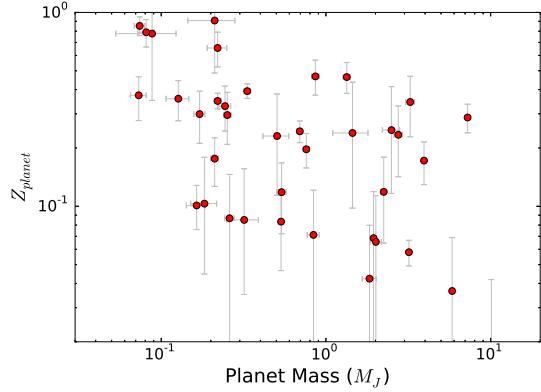


FIG. 8.— The heavy element fraction of planets as a function of mass. We observe a downward trend with a fair amount of spread. Compare especially with Figure 9, which shows the same value relative to the parent star.

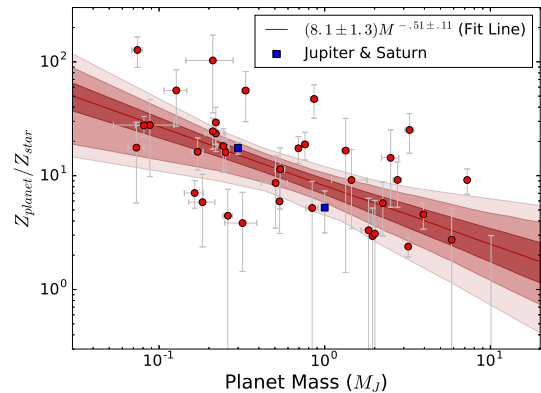


FIG. 9.— The heavy element enrichment of planets relative to their parent stars as a function of mass. The line is our median fit to the distribution from bootstrapping, with 1, 2, and 3  $\sigma$  error contours. Jupiter and Saturn are shown in blue, from Guillot (1999). The pattern appears to be moderately stronger than considering  $Z_{\text{planet}}$  alone against mass.

their cores are probably not especially massive) the envelopes of these planets are strongly metal-enriched, a result which can be further tested through spectroscopy. Note that we cal-

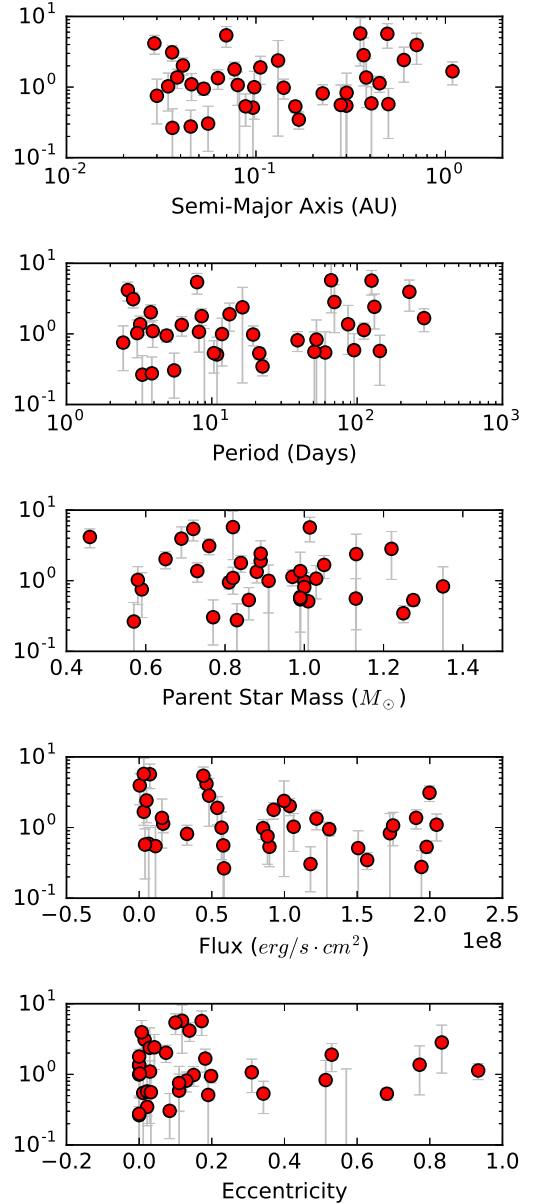


FIG. 10.— The relative residuals (calculated/fit) to the fit of  $Z_{\text{planet}}/Z_{\text{star}}$  against mass, plotted against the semi-major axis, period, parent star mass, flux, and eccentricity. No relation is apparent. The lack of a residual against flux implies that we have successfully cut out the inflated hot Jupiters; had we not, the high flux planets would be strong lower outliers.

culate our values of  $Z_{\text{star}}$  by assuming that stellar metal scales with the measured iron metallicity  $[\text{Fe}/\text{H}]$ . Considering other measurements of stellar metals in the future would be illuminating. For instance, since oxygen is a dominant component of both water and rock, perhaps there exists a tighter correspondence between  $Z_{\text{planet}}$  and the abundance of stellar oxygen, rather than with stellar iron.

We also considered the possibility that orbital properties might relate to the metal content, perhaps as a proxy for the migration history. We plot the residual from our mass vs.  $Z_{\text{planet}}/Z_{\text{star}}$  fit against the semi-major axis, period, eccentricity, and parent star mass in Figure 10. No pattern is evident for any of these. Given the number of planets and the size of our error-bars in our sample, we cannot rule out that any such

patterns exist, but we do not observe them here. We also considered the residual against the stellar flux. Any giant planets with radius inflation which had made it into our sample would appear as strong outliers below the fit, since we would have mistaken inflation for lower heavy element masses. Therefore, the lack of a pattern here suggests our flux cut is eliminating the inflated hot Jupiters as intended.

#### 5.4. Heavy Element Masses in Massive Planets

The extreme values for some of the heavy element masses are noteworthy. HAT-P-20 b, the upper-right point in Figure 5, contains over  $600 M_{\oplus}$  of metal. It is a  $7.2 M_J$  planet orbiting a metal-rich star ( $[\text{Fe}/\text{H}] = .35 \pm 0.08$ ), so we expect it would be metal-rich. Still, it is surprising that a planetary nebula can have so much metal to put into just one planet. This is not a high estimate; our choice of a  $10 M_{\oplus}$  core yields a value lower than if more of the metal were located in a core (see §3.1). A core-dominated equivalent could have as much as  $1000 M_{\oplus}$  of metal. As such, it is much more plausible that the planet is envelope-dominated. This planet, and its less dramatic brethren, raise questions about how such extreme objects can form (see also Leconte et al. (2009) for a similar discussion for other massive giant planets). These planets would have had to migrate through their system in such a way as to accumulate nearly all of the metal available in the disk.

However, in contrast with HAT-P-20b is Kepler-75b, at  $10.1 M_J$ , our most massive planet in the sample. It's metal-enrichment is significantly smaller than HAT-P-20b. One could entertain the suggestion that HAT-P-20b formed via core-accretion, but that Kepler-75b is a low-mass brown dwarf that formed through a different mechanism. At any rate, the future of determining whether a given object is a planet or low mass brown dwarf via characteristics like composition, rather than mass, which we advocate (and see also Chabrier et al. 2014) is promising.

## 6. DISCUSSION AND CONCLUSIONS

There is a strong connection between planet mass and metal content. From a sample of 38 transiting gas giants, we find that the heavy element mass increases as  $\sqrt{M}$ , so  $Z_{\text{planet}}$  decreases as  $1/\sqrt{M}$ . We also see that our planets are consistently enriched relative to their parent stars, and that they have a minimum  $M_z$  of  $5\text{-}10 M_{\oplus}$ . These results all support the core-accretion model of planet formation and the previous results from MF2011 that metal-enrichment is a defining characteristic of giant planets.

This work suggests that spectroscopy of the atmospheres of gas giants should also yield metal-enrichments compared to parent star abundances (Fortney et al. 2008), as is seen in the solar system. We suggest that this growing group of  $< 1000$  K planets should be a sample of great interest for atmospheric observations with the *James Webb Space Telescope*. Since the bulk metallicity of the cool planets can be determined, atmospheric studies to determine metal-enrichments can be validated. For most of our planets more massive than Saturn, the heavy elements values are high enough that most metals are in the envelope, rather than the core (See Figure 5), so our  $Z_{\text{planet}}$  values are upper limits on  $Z_{\text{atmosphere}}$ . Atmospheric observations to retrieve the mixing ratios of abundant molecules like  $\text{H}_2\text{O}$ ,  $\text{CO}$ ,  $\text{CO}_2$ , and  $\text{CH}_4$  could show if most heavy elements are found within giant planet envelopes or within cores. In comparison, for hot Jupiters  $> 1000$  K we cannot estimate with confidence the planetary bulk metal enrichment since the

radius inflation power is unknown.

Some connection between planetary heavy element mass and stellar metallicity is suggested by our work, but the correlation is not strong. A fruitful area of future investigation will be in analyzing stellar abundances other than iron. Learning which stellar metals most strongly correlate with planetary bulk metallicity (for instance, Fe, Mg, Si, Ni, O, C) would hint at the composition of planetary heavy elements and could provide insights into the planet formation process. With the continued success of ground-based transit surveys, along with K2 (Howell et al. 2014), and the 2017 launch of *TESS*, we expect to see many more "cooler" gas giant planets amenable to this type of analysis, which will continue to provide an excellent opportunity for further exploring these relations. With this continuing work on bulk metal-enrichment of planets, and the spectroscopy of planetary atmospheres, the move towards understanding planet formation in the mass / semi-major axes / composition planes should be extremely fruitful.

TABLE 1

#	Name	Mass ( $M_J$ )	Radius ( $R_J$ )	Age (Gyr)	Flux ( $\frac{10^6 \text{ erg}}{\text{cm}^2 \cdot \text{s}}$ )	[Fe/H] (Dex)	Metal Mass ( $M_{\oplus}$ )	$Z_p/Z_s$
1	CoRoT-8 b	$0.22 \pm 0.03$	$0.57 \pm 0.02$	0.1–3.0	$1.22 \cdot 10^8$	$0.30 \pm 0.10$	$45.92^{+7.22}_{-6.83}$	$23.51^{+7.30}_{-7.20}$
2†	CoRoT-9 b	$0.84 \pm 0.07$	$1.05 \pm 0.04$	1.0–8.0	$6.59 \cdot 10^6$	$-0.01 \pm 0.06$	$18.83^{+13.02}_{-18.83}$	$5.16^{+3.66}_{-3.16}$
3	CoRoT-10 b	$2.75 \pm 0.16$	$0.97 \pm 0.07$	0.1–3.0	$5.38 \cdot 10^7$	$0.26 \pm 0.07$	$201.79^{+82.92}_{-78.31}$	$9.06^{+4.03}_{-3.84}$
4	CoRoT-24 c	$0.09 \pm 0.04$	$0.44 \pm 0.04$	8.0–14.0	$5.67 \cdot 10^7$	$0.30 \pm 0.15$	$21.73^{+9.43}_{-8.18}$	$27.82^{+18.98}_{-18.01}$
5	GJ 436 b	$0.07 \pm 0.01$	$0.37 \pm 0.02$	0.5–10.0	$4.63 \cdot 10^7$	$-0.32 \pm 0.12$	$20.06^{+1.69}_{-1.62}$	$127.28^{+37.92}_{-37.81}$
6	HAT-P-11 b	$0.08 \pm 0.01$	$0.42 \pm 0.01$	2.4–12.4	$1.31 \cdot 10^8$	$0.31 \pm 0.05$	$20.36^{+1.93}_{-2.37}$	$27.66^{+5.32}_{-5.47}$
7	HAT-P-12 b	$0.21 \pm 0.01$	$0.96^{+0.03}_{-0.02}$	0.5–4.5	$1.91 \cdot 10^8$	$-0.29 \pm 0.05$	$11.86^{+3.15}_{-3.24}$	$24.63^{+7.27}_{-7.44}$
8†	HAT-P-15 b	$1.95 \pm 0.07$	$1.07 \pm 0.04$	5.2–9.3	$1.51 \cdot 10^8$	$0.22 \pm 0.08$	$42.39^{+30.80}_{-42.39}$	$2.95^{+2.21}_{-2.95}$
9	HAT-P-17 b	$0.53 \pm 0.02$	$1.01 \pm 0.03$	4.5–11.1	$8.97 \cdot 10^7$	$0.00 \pm 0.08$	$14.23^{+6.62}_{-6.30}$	$5.99^{+3.00}_{-2.88}$
10	HAT-P-18 b	$0.18^{+0.03}_{-0.03}$	$0.95 \pm 0.04$	6.0–16.8	$1.18 \cdot 10^8$	$0.10 \pm 0.08$	$6.10^{+4.39}_{-3.29}$	$5.95^{+4.56}_{-3.55}$
11	HAT-P-20 b	$7.25 \pm 0.19$	$0.87 \pm 0.03$	2.9–12.4	$2.00 \cdot 10^8$	$0.35 \pm 0.08$	$662.67^{+11.93}_{-109.30}$	$9.18^{+2.31}_{-2.28}$
12	HAT-P-54 b	$0.76 \pm 0.03$	$0.94 \pm 0.03$	1.8–8.2	$1.04 \cdot 10^8$	$-0.13 \pm 0.08$	$47.50^{+9.53}_{-9.38}$	$18.82^{+5.19}_{-5.14}$
13	HATS-6 b	$0.32 \pm 0.07$	$1.00 \pm 0.02$	0.1–13.7	$5.84 \cdot 10^7$	$0.20 \pm 0.09$	$8.62^{+6.88}_{-4.70}$	$3.83^{+3.27}_{-2.33}$
14	HATS-17 b	$1.34 \pm 0.07$	$0.78 \pm 0.06$	0.8–3.4	$9.97 \cdot 10^7$	$0.30 \pm 0.39$	$197.35^{+35.89}_{-33.39}$	$16.61^{+13.24}_{-13.20}$
15	HD 17156 b	$3.19 \pm 0.03$	$1.09 \pm 0.01$	2.4–3.8	$1.98 \cdot 10^8$	$0.24 \pm 0.05$	$58.84^{+9.02}_{-8.81}$	$2.38^{+0.46}_{-0.45}$
16	HD 80606 b	$3.94 \pm 0.11$	$0.98 \pm 0.03$	1.7–7.6	$1.65 \cdot 10^7$	$0.43 \pm 0.03$	$215.25^{+53.02}_{-52.16}$	$4.56^{+1.17}_{-1.16}$
17	KOI-372 b	$3.25 \pm 0.20$	$0.88 \pm 0.09$	0.4–1.6	$7.38 \cdot 10^6$	$-0.01 \pm 0.07$	$358.85^{+126.88}_{-119.99}$	$25.39^{+9.99}_{-9.55}$
18	Kepler-9 b	$0.25 \pm 0.01$	$0.84 \pm 0.07$	2.0–4.0	$8.53 \cdot 10^7$	$0.12 \pm 0.04$	$23.72^{+7.26}_{-6.97}$	$16.04^{+5.20}_{-5.01}$
19	Kepler-9 c	$0.17 \pm 0.01$	$0.82 \pm 0.07$	2.0–4.0	$3.29 \cdot 10^7$	$0.12 \pm 0.04$	$16.24^{+4.79}_{-4.63}$	$16.19^{+5.15}_{-5.00}$
20*	Kepler-16 b	$0.33 \pm 0.02$	$0.75 \pm 0.003$	0.5–10.0	$4.19 \cdot 10^5$	$-0.30 \pm 0.20$	$41.51^{+3.63}_{-2.78}$	$55.90^{+2.02}_{-26.15}$
21†	Kepler-30 c	$2.01 \pm 0.16$	$1.10 \pm 0.04$	0.2–3.8	$1.12 \cdot 10^7$	$0.18 \pm 0.27$	$42.35^{+30.65}_{-42.35}$	$3.13^{+2.99}_{-3.13}$
22	Kepler-30 d	$0.07 \pm 0.01$	$0.79 \pm 0.04$	0.2–3.8	$4.05 \cdot 10^6$	$0.18 \pm 0.27$	$8.70^{+1.95}_{-2.04}$	$17.70^{+11.86}_{-11.92}$
23*	Kepler-34 b	$0.22^{+0.01}_{-0.01}$	$0.76^{+0.01}_{-0.01}$	5.0–6.0	$3.21 \cdot 10^6$	$-0.07 \pm 0.15$	$24.40^{+2.00}_{-1.91}$	$29.29^{+10.50}_{-10.46}$
24*	Kepler-35 b	$0.13 \pm 0.02$	$0.73 \pm 0.01$	8.0–12.0	$5.06 \cdot 10^6$	$-0.34 \pm 0.20$	$14.49^{+2.66}_{-2.44}$	$56.11^{+29.18}_{-28.89}$
25	Kepler-45 b	$0.51 \pm 0.09$	$0.96 \pm 0.11$	0.4–1.5	$8.83 \cdot 10^7$	$0.28 \pm 0.14$	$37.31^{+23.19}_{-17.46}$	$8.71^{+6.30}_{-5.19}$
26†	Kepler-75 b	$10.10 \pm 0.40$	$1.05 \pm 0.03$	3.4–9.7	$1.29 \cdot 10^8$	$0.30 \pm 0.12$	$0.00^{+134.09}_{-0.00}$	$0.00^{+2.44}_{-0.00}$
27	Kepler-89 d	$0.16^{+0.02}_{-0.02}$	$0.98 \pm 0.01$	3.7–4.2	$1.57 \cdot 10^8$	$0.01 \pm 0.04$	$5.29^{+1.24}_{-1.10}$	$7.08^{+2.00}_{-1.87}$
28†	Kepler-117 c	$1.84 \pm 0.18$	$1.10 \pm 0.04$	3.9–6.7	$5.79 \cdot 10^7$	$-0.04 \pm 0.10$	$24.74^{+22.19}_{-24.74}$	$3.31^{+3.08}_{-3.31}$
29*	Kepler-413 b	$0.21^{+0.07}_{-0.07}$	$0.39 \pm 0.01$	0.5–10.0	$3.20 \cdot 10^6$	$-0.20 \pm 0.20$	$60.77^{+21.96}_{-20.96}$	$102.59^{+68.79}_{-67.18}$
30	Kepler-419 b	$2.50 \pm 0.30$	$0.96 \pm 0.12$	1.6–4.1	$4.81 \cdot 10^7$	$0.09 \pm 0.15$	$195.99^{+129.47}_{-99.18}$	$14.32^{+10.81}_{-8.94}$
31	Kepler-420 b	$1.45 \pm 0.35$	$0.94 \pm 0.12$	6.3–12.3	$1.57 \cdot 10^7$	$0.27 \pm 0.09$	$109.62^{+85.87}_{-59.24}$	$9.12^{+7.71}_{-5.72}$
32†	Kepler-432 b	$5.84 \pm 0.05$	$1.10 \pm 0.03$	2.6–4.2	$1.73 \cdot 10^8$	$-0.02 \pm 0.06$	$67.29^{+59.85}_{-67.29}$	$2.71^{+2.44}_{-2.71}$
33	WASP-8 b	$2.24^{+0.08}_{-0.09}$	$1.04^{+0.01}_{-0.05}$	3.0–5.0	$1.75 \cdot 10^8$	$0.17 \pm 0.07$	$84.30^{+43.53}_{-38.35}$	$5.71^{+3.09}_{-2.76}$
34	WASP-29 b	$0.24 \pm 0.02$	$0.79^{+0.06}_{-0.04}$	7.0–13.0	$2.05 \cdot 10^8$	$0.11 \pm 0.14$	$25.40^{+6.60}_{-6.14}$	$18.23^{+7.68}_{-7.48}$
35	WASP-59 b	$0.86 \pm 0.04$	$0.78 \pm 0.07$	0.1–1.2	$4.41 \cdot 10^7$	$-0.15 \pm 0.11$	$128.21^{+26.64}_{-25.11}$	$47.16^{+15.65}_{-15.30}$
36†	WASP-69 b	$0.26 \pm 0.02$	$1.06 \pm 0.05$	0.5–4.0	$1.94 \cdot 10^8$	$0.14 \pm 0.08$	$7.18^{+4.91}_{-7.18}$	$4.46^{+3.16}_{-4.46}$
37	WASP-80 b	$0.54^{+0.04}_{-0.04}$	$1.00^{+0.03}_{-0.03}$	0.5–10.0	$1.06 \cdot 10^8$	$-0.13^{+0.15}_{-0.17}$	$20.36^{+8.22}_{-7.78}$	$11.47^{+6.14}_{-6.32}$
38	WASP-84 b	$0.69 \pm 0.03$	$0.94 \pm 0.02$	0.4–1.4	$9.26 \cdot 10^7$	$0.00 \pm 0.10$	$53.69^{+6.86}_{-6.60}$	$17.39^{+4.63}_{-4.59}$

NOTE. — A \* indicates circumbinary planets. A † indicates those planets with results adjusted to reflect the fact that a certain portion of their samples could not be modeled (see §4 for discussion). Sources – 1: Bordé et al. (2010a), 2: Deeg et al. (2010), 3: Bonomo et al. (2010), 4: Bordé et al. (2010b), 5: Bean et al. (2006), Southworth (2010), 6: Bakos et al. (2010), 7: Hartman et al. (2009), 8: Kovács et al. (2010), 9: Howard et al. (2012), 10: (Hartman et al. 2011), 11: Bakos et al. (2011), 12: Bakos et al. (2015), 13: Hartman et al. (2015), 14: Brahm et al. (2015), 15: Nutzman et al. (2011), 16: Pont et al. (2009) & Naef et al. (2001) & Saffe et al. (2005), 17: Mancini et al. (2015), 18: Holman et al. (2010), 19: Holman et al. (2010), 20: Doyle et al. (2011), 21: Sanchis-Ojeda et al. (2012), 22: Sanchis-Ojeda et al. (2012), 23: Welsh et al. (2012), 24: Welsh et al. (2012), 25: Johnson et al. (2012), 26: Bonomo et al. (2015), 27: Masuda et al. (2013) & Hirano et al. (2012), 28: Bruno et al. (2015), 29: Kostov et al. (2014), 30: Dawson et al. (2014) & Dawson et al. (2012), 31: Santerne et al. (2014), 32: Ortiz et al. (2015), 33: Queloz et al. (2010), 34: Heller et al. (2010), 35: Hébrard et al. (2013), 36: Anderson et al. (2014), 37: TriAUD et al. (2015), 38: Anderson et al. (2014)

## REFERENCES

- Akeson, R. L., et al. 2013, *PASP*, 125, 989
- Alibert, Y., Mousis, O., Mordasini, C., & Benz, W. 2005, *ApJ*, 626, L57
- Anderson, D. R., et al. 2014, *MNRAS*, 445, 1114
- Bakos, G. Á., et al. 2010, *ApJ*, 710, 1724
- 2011, *ApJ*, 742, 116
- 2015, *AJ*, 149, 149
- Baraffe, I., Chabrier, G., & Barman, T. 2008, *A&A*, 482, 315
- Baraffe, I., Chabrier, G., Fortney, J., & Sotin, C. 2014, *Protostars and Planets VI*, 763
- Barman, T. S., Konopacky, Q. M., Macintosh, B., & Marois, C. 2015, *ApJ*, 804, 61
- Bean, J. L., Benedict, G. F., & Endl, M. 2006, *ApJ*, 653, L65
- Bonomo, A. S., et al. 2010, *A&A*, 520, A65
- 2015, *A&A*, 575, A85
- Bordé, P., et al. 2010a, *A&A*, 520, A66
- 2010b, *A&A*, 520, A66
- Brahm, R., et al. 2015, *ArXiv e-prints*
- Bruno, G., et al. 2015, *A&A*, 573, A124
- Burrows, A., Hubeny, I., Budaj, J., & Hubbard, W. B. 2007, *ApJ*, 661, 502
- Chabrier, G., Johansen, A., Janson, M., & Rafikov, R. 2014, *Protostars and Planets VI*, 619
- Dawson, R. I., Johnson, J. A., Morton, T. D., Crepp, J. R., Fabrycky, D. C., Murray-Clay, R. A., & Howard, A. W. 2012, *ApJ*, 761, 163
- Dawson, R. I., et al. 2014, *ApJ*, 791, 89
- Deeg, H. J., et al. 2010, *Nature*, 464, 384
- Demory, B.-O., & Seager, S. 2011, *ApJS*, 197, 12
- Doyle, L. R., et al. 2011, *Science*, 333, 1602
- Fischer, D. A., & Valenti, J. 2005, *ApJ*, 622, 1102
- Fletcher, L. N., Orton, G. S., Teanby, N. A., Irwin, P. G. J., & Bjoraker, G. L. 2009, *Icarus*, 199, 351
- Fortney, J. J., Marley, M. S., & Barnes, J. W. 2007, *ApJ*, 659, 1661
- Fortney, J. J., Marley, M. S., Saumon, D., & Lodders, K. 2008, *ApJ*, 683, 1104
- Fortney, J. J., Mordasini, C., Nettelmann, N., Kempton, E. M.-R., Greene, T. P., & Zahnle, K. 2013, *ApJ*, 775, 80
- Fortney, J. J., & Nettelmann, N. 2010, *Space Sci. Rev.*, 152, 423
- Guillot, T. 1999, *Planet. Space Sci.*, 47, 1183
- 2010, *A&A*, 520, A27
- Guillot, T., Santos, N. C., Pont, F., Iro, N., Melo, C., & Ribas, I. 2006, *A&A*, 453, L21
- Hartman, J. D., et al. 2009, *ApJ*, 706, 785
- 2011, *ApJ*, 726, 52
- 2015, *AJ*, 149, 166
- Hébrard, G., et al. 2013, *A&A*, 549, A134
- Helled, R., & Bodenheimer, P. 2014, *arXiv:1404.5018*
- Hellier, C., et al. 2010, *ApJ*, 723, L60
- Hirano, T., et al. 2012, *ApJ*, 759, L36
- Holman, M. J., et al. 2010, *Science*, 330, 51
- Howard, A. W., et al. 2012, *ApJ*, 749, 134
- Howell, S. B., et al. 2014, *PASP*, 126, 398
- Ida, S., & Lin, D. N. C. 2004, *ApJ*, 604, 388
- Johnson, J. A., et al. 2012, *AJ*, 143, 111
- Klahr, H., & Bodenheimer, P. 2006, *ApJ*, 639, 432
- Konopacky, Q. M., Barman, T. S., Macintosh, B. A., & Marois, C. 2013, *Science*, 339, 1398
- Kostov, V. B., et al. 2014, *ApJ*, 784, 14
- Kovács, G., et al. 2010, *ApJ*, 724, 866
- Kreidberg, L., et al. 2014, *ApJ*, 793, L27
- Leconte, J., Baraffe, I., Chabrier, G., Barman, T., & Levrard, B. 2009, *A&A*, 506, 385
- Lissauer, J. J., Hubickyj, O., D'Angelo, G., & Bodenheimer, P. 2009, *Icarus*, 199, 338
- Lodders, K. 2009, *arXiv:0910.0811*
- Lopez, E. D., & Fortney, J. J. 2014, *ApJ*, 792, 1
- Madhusudhan, N., Mousis, O., Johnson, T. V., & Lunine, J. I. 2011, *ApJ*, 743, 191
- Mancini, L., et al. 2015, *ArXiv e-prints*
- Marley, M. S., Fortney, J. J., Hubickyj, O., Bodenheimer, P., & Lissauer, J. J. 2007, *ApJ*, 655, 541
- Masuda, K., Hirano, T., Taruya, A., Nagasawa, M., & Suto, Y. 2013, *ApJ*, 778, 185
- Miller, N., & Fortney, J. J. 2011, *ApJ*, 736, L29
- Miller, N., Fortney, J. J., & Jackson, B. 2009, *ApJ*, 702, 1413
- Mordasini, C., Alibert, Y., Benz, W., Klahr, H., & Henning, T. 2012, *A&A*, 541, A97
- Mordasini, C., Klahr, H., Alibert, Y., Miller, N., & Henning, T. 2014, *A&A*, 566, A141
- Naef, D., et al. 2001, *A&A*, 375, L27
- Nutzman, P., et al. 2011, *ApJ*, 726, 3
- Öberg, K. I., Murray-Clay, R., & Bergin, E. A. 2011, *ApJ*, 743, L16
- Ortiz, M., et al. 2015, *A&A*, 573, L6
- Pollack, J. B., Hubickyj, O., Bodenheimer, P., Lissauer, J. J., Podolak, M., & Greenzweig, Y. 1996, *Icarus*, 124, 62
- Pont, F., et al. 2009, *A&A*, 502, 695
- Queloz, D., et al. 2010, *A&A*, 517, L1
- Saffe, C., Gómez, M., & Chavero, C. 2005, *A&A*, 443, 609
- Sanchis-Ojeda, R., et al. 2012, *Nature*, 487, 449
- Santerne, A., et al. 2014, *A&A*, 571, A37
- Saumon, D., Chabrier, G., & van Horn, H. M. 1995, *ApJS*, 99, 713
- Schneider, J., Dedieu, C., Le Sidaner, P., Savalle, R., & Zolotukhin, I. 2011, *A&A*, 532, A79
- Southworth, J. 2010, *MNRAS*, 408, 1689
- Southworth, J., Wheatley, P. J., & Sams, G. 2007, *MNRAS*, 379, L11
- Spiegel, D. S., & Burrows, A. 2013, *ApJ*, 772, 76
- Thompson, S. L. 1990, *ANEOS—Analytic Equations of State for Shock Physics Codes*, Sandia Natl. Lab. Doc. SAND89-2951
- Triaud, A. H. M. J., et al. 2015, *MNRAS*, 450, 2279
- Weiss, L. M., et al. 2013, *ApJ*, 768, 14
- Welsh, W. F., et al. 2012, *Nature*, 481, 475
- Wong, M. H., Mahaffy, P. R., Atreya, S. K., Niemann, H. B., & Owen, T. C. 2004, *Icarus*, 171, 153
- Zapolsky, H. S., & Salpeter, E. E. 1969, *ApJ*, 158, 809